Available online at www.sciencedirect.com
ScienceDirect
Trans. Nonferrous Met. Soc. China 34(2024) 1167−1177
Transactions of Nonferrous Metals Society of China
www.tnmsc.cn

A novel creep model with synergetic Orowan bypassing and climbing mechanisms in nickel-base superalloys

Fang LI[1], Ding-ling YUAN[2], Kang-hua CHEN[1,2], Song-yi CHEN[2], Li LI[3]

1. State Key Laboratory of Powder Metallurgy, Central South University, Changsha 410083, China;
2. Light Alloy Research Institute, Central South University, Changsha 410083, China;
3. State Key Laboratory of Advanced Design and Manufacturing for Vehicle Body, College of Mechanical and Vehicle Engineering, Hunan University, Changsha 410082, China

Received 25 July 2022; accepted 27 February 2023

Abstract: A novel creep model was proposed to accurately and conveniently predict the steady-state creep rate of precipitation-strengthening nickel-base superalloys. Based on the space distribution of precipitates, the synergetic mode of Orowan bypassing and dislocation climbing mechanisms in dislocation−precipitate interaction was coupled into the new creep model according to probability−correlative method. The results show that the new model can accurately describe the steady-state creep rate compared with the experimental data, which is far better than the classical model. Moreover, the present model no longer relies on the adjustable parameters. The quantitative relationship between threshold stress and temperature is also determined. This work sheds new light on the dislocation−precipitate interaction during creep deformation, and provides an effective model for designing precipitation-strengthening alloys with improved creep properties.

Key words: nickel-base superalloys; creep model; steady-state creep rate; threshold stress

1 Introduction

Ni-based superalloys for their application in aero engines and other modern turbine engines have been developed over the last several decades, owing to their excellent resistance to high-temperature creep, great tensile strength, and prominent fatigue properties [1−4]. The exceptional properties of Ni-based superalloys derive from the distinctive microstructures, which comprise the fine $L1_2$ precipitates of Ni_3(Al,Ti), and the face-centred-cubic (fcc) matrix [5−7]. With the increasing demand for extending the service life of superalloys at high temperatures, the traditional methods calculating the creep rate fail to meet the present need. Hence, it is critical to understand the relationship between microstructure and the steady-state creep rate in depth and establish a new physics-based model, to improve the experimental scheme and design the Ni-based superalloys with long service life.

In recent years, to better understand the creep mechanism of metals and alloys, many methods have been developed to reveal physically meaningful behaviors on a macroscopic scale and explicate the unclear experiments [8,9]. For instance, a model based creep equation for the creep deformation behavior of dispersion strengthened superalloys is developed to describe the strong impact of temperature and stress on the creep rate, which considers the thermal activation of the dislocation detachment from attractive oxide particles [10]. According to the empirical creep

Corresponding author: Song-yi CHEN, Tel: +86-15874285082, E-mail: Sychen08@csu.edu.cn;
Li LI, Tel: +86-15675147443, E-mail: tonylili@hnu.edu.cn
DOI: 10.1016/S1003-6326(23)66461-1

model, the steady-state creep rate (minimum creep rate or secondary creep rate) is a function of temperature and stress, which is determined by fitting experimental creep data [11]. However, to get insight into the relation between microstructural factors and the minimum creep rate, the influence of the stacking fault energy [12], the grain size [13] and the morphology of precipitates [14] on minimum creep rate has been discovered. Besides, a modified creep model considering the effect of bimodal precipitate-distributions is established, and the predictions are compared with the experimental results in multimodal nickel-base superalloys [15]. The above methods are practically suitable for the prediction of experimental creep rate, but some parameter values can only be decided by fitting experimental data. However, the development of new alloys is limited if the experimental data are not obtainable for those new alloys.

As is known to all, general approaches to increase the plastic deformation resistance of metals and alloys include solid solution strengthening, precipitation strengthening and cold working process. Moreover, the precipitation hardening is considered as the most effective way to enhance the creep property of high temperature metallic materials [16]. To analyze the effect of precipitates strengthening on creep strength, the constant threshold stress is frequently introduced into the creep rate equation [17]. Although the Orowan mechanism is used to evaluate the influence of precipitates on the threshold stress, it generally makes for an overmeasure of the contribution of precipitates, due to dislocations could climb across the precipitations at elevated temperatures [18]. Furthermore, according to the theory of lattice self-diffusion commanding the dislocation climb process, the dislocation climb creep model is developed to quantitatively estimate the influences of temperature, interface effect and nanoparticle size on the activation energy and threshold stress. This method arrives at the ratio of threshold stress to Orowan stress ranging from 0.4 to 0.5, and the activation energies from 260 to 300 kJ/mol [19]. On the other hand, the threshold stress as low as 0.02−0.06 of the Orowan stress is eventually predicted based on the local climb assumption presented by ARZT and ASHBY [20]. However, the threshold stress calculated by the above methods heavily depends on the fitting parameters, which is inconvenient to be popularized to the other system alloys.

The purpose of the current research is to develop a new creep model that considers microstructures and does not need further to experimentally measure the creep properties of the alloys. Moreover, our creep model takes into account the effect of the precipitation strengthening on the steady-state creep rate and calculates the threshold stress. Simultaneously, the radius distribution and the relative position between the dislocation bypasses plane and precipitation center are considered in the calculation of the contribution from precipitations to the creep threshold stress. Hence, considering coexistence of climb and Orowan mechanisms, the present physics-based model can provide insights for accurate and effective design of long-service life alloys under complex conditions.

2 Theory and model

2.1 Steady-state creep rate modelling

Dislocations work as the effective barrier to the motion of other dislocations. Due to the non-negligible effect of dislocation on the creep rate, it is necessary to understand the evolution of the dislocation density. The dislocation source will generate new dislocations during the work hardening process, while at the same time dislocations with opposite sign will be eliminated due to recovery process. The generated dislocations will strengthen the material, and also the recovery process will soften the material. According to the classical recovery model for creep, work hardening and recovery can be expressed as the following equation [21,22]:

$$\frac{\mathrm{d}\rho}{\mathrm{d}\varepsilon}=\frac{m}{bL}-2\tau_{\mathrm{L}}M(T,\sigma)\rho^{2}/\dot{\varepsilon} \tag{1}$$

where ρ is the dislocation density, ε is the plastic strain, m is the Tayor factor and L is the spurt distance when the dislocation is released during deformation. b is the magnitude of Burger's vector, $\tau_{\mathrm{L}}(=Gb^2/2)$ is the dislocation line tension, G is the shear modulus, $M(T, \sigma)$ is the dislocation mobility function, T the temperature, σ the stress and $\dot{\varepsilon}$ the strain rate. The two terms on the right-hand side of the equation take the Orowan's expression for the work hardening and the static recovery term into

account. The dislocation density increases rapidly in the initial stage of creep test in Ni-based superalloys, indicating that the work hardening term is the dominant deformation mechanism in this stage. However, the dislocation density reaches the equilibrium with increasing the strain because of the dislocation annihilating during the recovery process. For equilibrium conditions where $d\rho/d\varepsilon=0$, the steady-state creep rate ($\dot{\varepsilon}_{sec}$) can be written as [22,23]

$$\dot{\varepsilon}_{sec}=\frac{2\tau_L bK}{\alpha_T m^2}M(T,\sigma_{disl})\left(\frac{\sigma_{disl}}{\alpha_T mGb}\right)^3 \tag{2}$$

where K is a constant, and α_T is the work hardening constant. The Taylor's equation is given by

$$\sigma_{disl}=\alpha_T mGb\rho^{1/2}=\sigma_{appl}-\sigma_i \tag{3}$$

where σ_{disl} is the stress on forest dislocations, and σ_{appl} is the applied stress. σ_i is the threshold stress, which is derived from the solid solution strengthening and the precipitation strengthening. In this work, only the precipitation strengthening is considered because the contribution of solid solution strengthening is relatively low [24,25].

The dislocation mobility can be expressed as

$$M(T,\sigma)=\frac{D_{0sd}b}{k_BT}\exp\left(\frac{\sigma b^3}{k_BT}\right)\cdot \exp\left\{-\frac{Q_{sd}}{R_gT}\left[1-\left(\frac{\sigma}{R_m}\right)^2\right]\right\}/f_{sol} \tag{4}$$

where D_{0sd} is the pre-exponential factor for self-diffusion, k_B is the Boltzmann's constant, Q_{sd} is the activation energy for self-diffusion, R_g is the molar gas constant, and R_m is the tensile strength at room temperature. f_{sol} a constant that takes the influence of elements in solid solution into account. $f_{sol}=\exp[Q_{sol}/(R_gT)]$, where Q_{sol} is the increase of activation energy due to element in solid solution.

2.2 Contribution from precipitation

In general, precipitation strengthening plays an important role in reducing the steady-state creep rate. The contribution from precipitation strengthening to the threshold stress is evaluated based on the Orowan bypass mechanism. The classical Orowan stress (σ_O) is expressed as

$$\sigma_O=0.8\frac{2\tau_L m}{b\lambda} \tag{5}$$

where λ is the interparticle spacing. $\lambda=r(2\pi/3f)^{1/2}$ where r is the precipitation radius and f is the precipitation volume fraction. σ_O is dependent on the temperature through shear modulus.

Many researches [22−25] have been conducted to calculate the threshold stress demanded by dislocation climb across the precipitation. The dislocation is attached to the precipitation when local climb happens. The threshold stress for the local climb is about half the Orowan stress [26]. In addition, when the dislocation is in connect with the precipitation at single points (general climb), the threshold stress is extremely small [27]. In fact, the latter case is more commonly accepted, even though it denotes that the dislocation freely climbs across the precipitation.

To find a way out of the dilemma, a new method will be applied in the present work. The following assumptions is made [28,29]:

(1) Because the threshold stress of climb mechanism is quite small compared to that of Orowan mechanism, it is the time for the dislocation climbing across the precipitations that decides whether a precipitation will be climbed or not.

(2) The maximum precipitation radius where there is sufficient time for dislocation to climb across precipitation is defined as the critical radius (r_{crit}). Therefore, when precipitation radius is larger than r_{crit}, the dislocation bypasses precipitation through Orowan bowing, which would produce the effective contribution to the creep threshold stress. Instead, there remains sufficient for dislocations to climb precipitation, which would not contribute to the creep threshold stress.

(3) The shear mechanism is not considered, because the dislocation is deemed to freely climb across small precipitation.

These assumptions have been used to predict the steady-state creep rate of the copper−cobalt alloys and the austenitic stainless steels. The predicted results are in good agreement with the experimental data [22,23,25].

The time for a dislocation to climb across a particle (t_{climb}) must be at least the glide time between the particles (t_{glide}). Hence, "$t_{climb}=t_{glide}$" can be used to evaluate the critical radius.

The climb time is given by the critical radius divided by the climb velocity (v_{climb}) of the dislocations, and the climb velocity is dependent on

the climb mobility [25]:

$$t_{\text{climb}}=\frac{2r_{\text{crit}}}{v_{\text{climb}}}=\frac{2r_{\text{crit}}}{M(T,\sigma_{\text{appl}})b\sigma_{\text{appl}}} \tag{6}$$

The glide time can be computed as the interparticle spacing divided by the glide velocity (v_{glide}) [23,30]:

$$t_{\text{glide}}=\frac{\lambda}{v_{\text{glide}}}=\lambda\frac{b\rho}{\dot{\varepsilon}_{\text{sec}}m} \tag{7}$$

By combing Eqs. (6) and (7), an expression of the critical radius can be given:

$$r_{\text{crit}}=2M(T,\sigma)b^2\sigma\lambda\frac{\rho}{\dot{\varepsilon}_{\text{sec}}m} \tag{8}$$

The steady-state creep rate, $\dot{\varepsilon}_{\text{sec}}$, on the right-hand side of Eq. (8) changes as a function of the displacement of climbing, which controls the value of r_{crit}. Hence, there is not a simple analytic solution for the critical radius.

2.3 Orowan synergetic bypassing and climbing mechanism

It was assumed that the interaction between dislocation and precipitate always occurs at the central plane of precipitate [30−32]. However, this assumption is not physically realistic. The experimental observation has demonstrated that the central plane of the precipitation is not always the interaction plane between the dislocation and the precipitation [33−35]. Therefore, the current study considers that the operative precipitation strengthening mechanism strongly relies on the relative location between the glide plane of dislocation and the precipitation center. A conclusion is drawn that not all precipitates larger than r_{crit} would contribute to the threshold stress.

As shown in Fig. 1, the Orowan mechanism works in Region OA ($r>r_{\text{crit}}$), which can produce effective contributions to the threshold stress, but in Region AB ($r<r_{\text{crit}}$), there is enough time for dislocations to climb precipitate, which would not contribute to the threshold stress. It is necessary to explain that the present work regarded the cuboidal precipitate as a circular shape in Ni-based superalloys for the simplification, due to the classical precipitate strengthening model assuming that all precipitates are circular in form [36,37]. Hence, a novel Orowan bypassing synergetic climbing mechanism is presented in nickel-based superalloys with the precipitate radius larger than r_{crit} based on the probabilistic statistical theory.

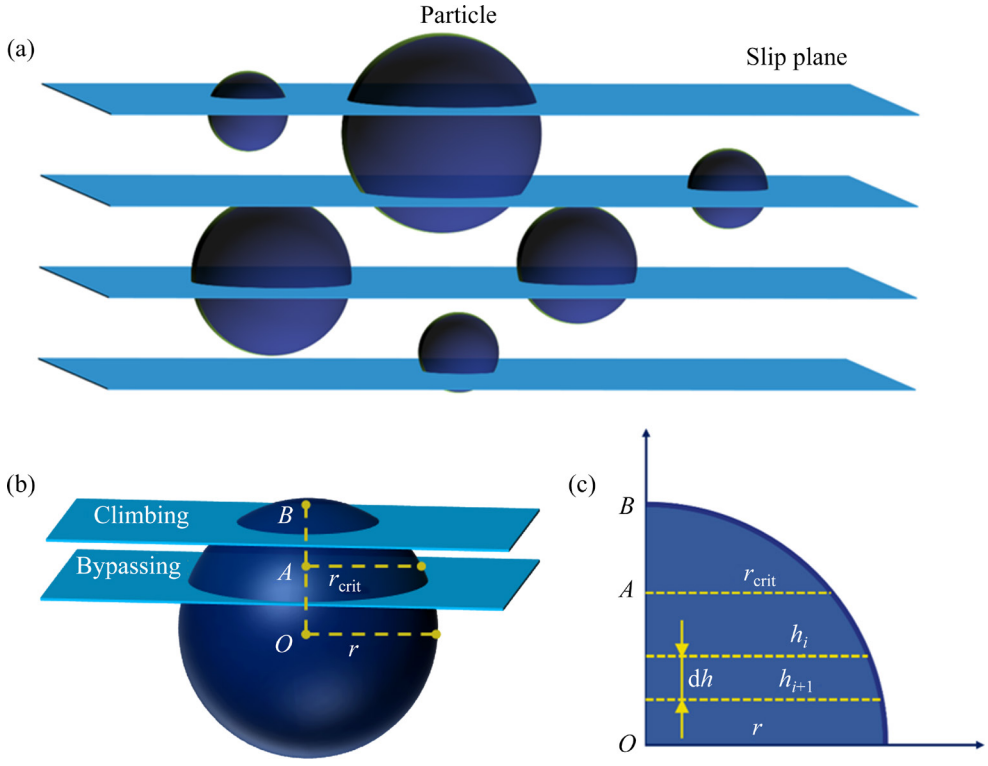

Fig. 1 Uncertainty of interaction patterns between dislocations and precipitates (a); Position relationship between dislocation bypass plane and precipitation center (b); Contributed strength from individual parts based on calculus method (c)

In Region *OA*, the occurrence probability of the occurrence of Orowan mechanism can be expressed as

$$p=\frac{l_{OA}}{r}=\sqrt{1-\left(\frac{r_{\text{crit}}}{r}\right)^2} \tag{9}$$

where l_{OA} is the distance of the interaction plane *OA*, and r is the radius of the precipitate.

The differential quadrature method is used to calculate the contribution of Orowan bypassing mechanism to the creep strength in the present research. As shown in Fig. 1(b), the *OA* region can be bisected into finite parts, denoted by n. With the consideration of probability effect, the contribution of Orowan bypassing mechanism to the creep strength (σ_{pre}) can be given by

$$\sigma_{\text{pre}}=\frac{1}{n}\sum_{i=1}^{n}\sigma_{\text{O}}(h_i),\ r_{\text{crit}}\le h_i \tag{10}$$

where $h_1=r_{\text{crit}}$, $h_{i+1}=\sqrt{r^2-[(r^2-h_i^2)^{1/2}-\text{d}h]^2}$, and $\text{d}h=l_{OA}/n$.

In the *AB* region, the contribution of precipitation to threshold stress is ineffective, owing to the dislocation can climb across the precipitation rather than bypass it through Orowan looping.

Hence, when the radius of given precipitation is larger than r_{crit}, considering the probability−correlative Orowan synergetic bypassing and climbing mechanism, the stress contributed by the precipitation ($\sigma_{\text{pre}}^{\text{p}}$) can be given by

$$\sigma_{\text{pre}}^{\text{p}}=p\sigma_{\text{pre}} \tag{11}$$

Many experiments show that the precipitate radius approximately meets the law of the lognormal distribution [25]. As shown in Fig. 2(b), the region of the precipitate-radius distribution consists of two regions, including the climbing region ($r<r_{\text{crit}}$) where the climbing mechanism occurs and the looping region ($r_{\text{crit}}<r$) where the Orowan bypassing synergetic climbing mechanism occurs. The exponential form can be expressed by

$$N_{\text{A}}=N_{\text{A0}}\exp(-kr_{\text{c}}) \tag{12}$$

where N_{A} is the number of precipitates larger than the precipitate radius r_{c}. k is a constant, which is relevant to the average precipitation radius: $k=1/r$. And, N_{A0} is the number of precipitates per unit area $N_{\text{A0}}=1/\lambda^2$.

Therefore, the average interparticle spacing

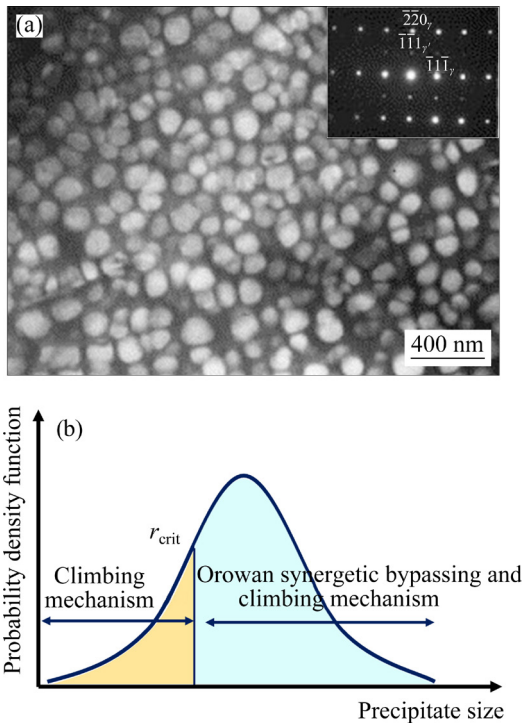

Fig. 2 Illustration of γ' precipitate in IN 738LC (a) [38]; Probability density function vs precipitate size (b)

(λ_{crit}) between particles is larger than r_{crit}, which can be expressed as

$$\lambda_{\text{crit}}=\sqrt{N_{\text{A0}}}\exp(kr_{\text{crit}}/2) \tag{13}$$

As the radius of precipitation follows an exponential distribution, and the average precipitate radius is larger than the critical radius, the radius of some precipitates may be smaller than the critical radius. This trend results in the fact that only a part of the precipitates can contribute to the threshold stress by Orowan looping. However, the other part of the precipitates less than the critical radius only makes an ineffective contribution, owing to the enough time for dislocation to climb across the precipitates. Moreover, the average precipitate spacing is a statistical constant in the previous theory, while it varies significantly with critical precipitate radius in the probability−correlative model. The probability−correlative Orowan mechanism is more effective and accurate than the classical Orowan mechanism, explaining the influence of precipitate radius probability distribution. Hence, the probability−correlative Orowan mechanism is necessary to more accurately assess the effect of particles on threshold stress, compared to the classic model.

As emphasized above, only the radius of precipitates greater than r_{crit} can contribute the threshold stress by Orowan mechanism. The new Orowan stress can be formulated as

$$\sigma_{pre}^{new}=\sigma_{pre}\exp(-kr_{crit}/2) \quad (14)$$

Here, the steady-state creep rate is calculated based on the iterative method. Under a certain applied stress, we first calculate the initial value of the threshold stress based on Eq. (5) with the parameters (b, m and G). Then, the initial steady creep rate is obtained by Eqs. (2)−(4). Subsequently, the initial steady state creep rate is brought into Eq. (8) to obtain initial critical radius of precipitate. By combining Eq. (5) and Eqs. (9)−(14), the new threshold stress is obtained and brought into Eq. (3) to calculate the final steady state creep rate. Finally, updating the applied stress with this cycle is need to calculate the new creep rate.

3 Comparison of model results with experiments

3.1 Validity of model

To verify the accuracy and rationality of the new creep model, the calculated results of the steady-state creep rate mentioned above are compared with the experimental results and calculated results from the Dyson creep theory [39−41]. Table 1 gives the chemical composition of the current nickel-base superalloys. According to the previous experimental results, the related parameters for calculating the steady-state creep rate are obtained from Table 2.

Figure 3(a) shows the steady-state creep rate of the nickel-base superalloys computed by the Dyson creep model, our creep model, and the experimental results in a broader range of applied stresses, respectively. At the temperatures of 850 and 950 °C, the predicted results of our model and Dyson model are in good agreement with experimental results. When the temperature reaches 750 °C, the steady-state creep rate predicted by the Dyson creep model is better than that of the present model. The Dyson

Table 1 Chemical composition of IN 738LC (wt.%)

Ni	Cr	Co	Mo	W	Ta
Bal.	16	8.5	2	2.6	1.8
Nb	Al	Ti	B	Zr	C
0.9	3.5	3.5	0.01	0.05	0.11

Table 2 Parameters used in model

Parameter	Value
Precipitate radius, r/nm	161
Volume fraction of precipitates, f	0.45
Magnitude of Burger's vector, b/m	2.5×10^{-10}
Taylor factor, m	3.06
Boltzmann's constant, k_B/(J·K^{-1})	1.381×10^{-23}
Work hardening constant, α_T	0.19
Shear modulus, G/MPa	78−(0.036(T−273))×10^3 (T−Temperature/°C)
Pre-exponential factor for self-diffusion, D_{0sd}/(m^2·s^{-1})	1.9×10^{-4}
Activation energy for self-diffusion, Q_{sd}/(J·mol^{-1})	2.84×10^5
Molar gas constant, R_g/(J·mol^{-1}·K^{-1})	8.314

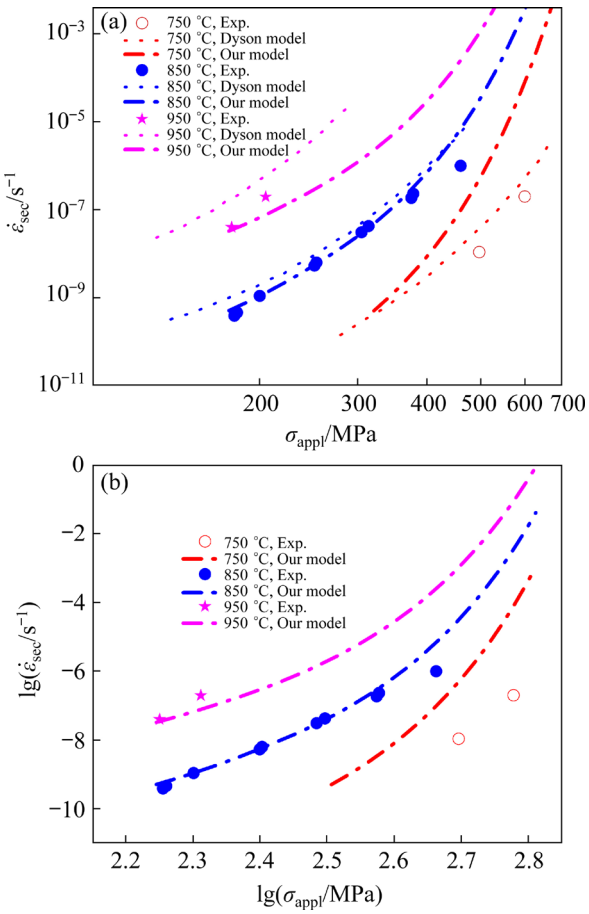

Fig. 3 Variation of steady-state creep rate ($\dot{\varepsilon}_{sec}$) with applied stress (σ_{appl}) from our model, Dyson creep model and previous experimental data at different temperatures (a); Comparison of $\lg\dot{\varepsilon}_{sec}$ as function of $\lg\sigma_{appl}$ between our model prediction and experimental data (b) [39−41]

model predicts creep properties in functional forms of not only stress and temperature but also microstructural factors (such as dislocation density, precipitate radius, inter-particle spacing of precipitates and volume fraction of precipitates). Although the Dyson model is practically suitable for analyses of experimental creep properties, some model parameter values should be determined by fitting the experimental creep data. The application to new alloys is limited if experimental information is not available. However, it is important to emphasize that our model proposed in this work does not involve any fitting parameters. Besides, the slope of the curve increases with the increase of applied stress, indicating the stronger effect on the steady-state creep rate with increasing the applied stress. This is because of an increasing difference between the threshold stress (the new Orowan stress) and the applied stress. Moreover, the stress exponent can be measured from the slope of plot in Fig. 3(b), which is a key parameter in previous theory. The stress exponents at low temperature/high stress are larger than those at high temperature/low stress, which is consistent with the previous conclusion [42].

The correlation between the threshold stress and applied stress based on Eq. (14) is illustrated in Fig. 4. The new Orowan stress increases in less speed with the applied stress increasing, which leads to the increase of the difference between the new Orowan stress and the applied stress. It is noted that the critical radius r_{crit} plays an important role in calculating the new Orowan stress. Because the critical radius decreases with increasing applied stress, the number of precipitates that can effectively contribute to threshold stress rises with the increase of applied stress. On the other hand, for the single precipitate whose radius is larger than the critical precipitate radius, the effective part of precipitation on threshold stress is positively correlated with the applied stress. Thus, the present theory is more convenient and accurate to be capable of capturing the main features of the variation in the steady-state creep rate increment with the increase of the applied stress.

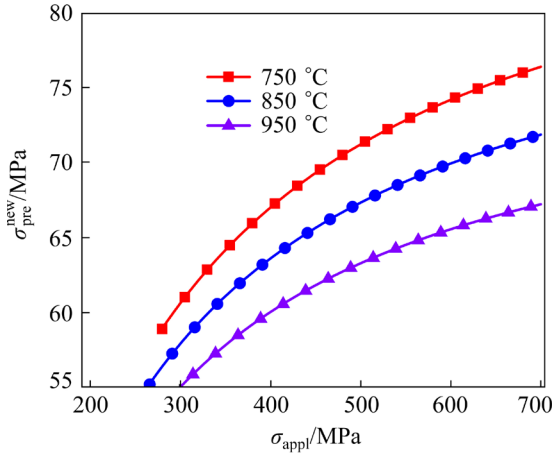

Fig. 4 Relationship between new Orowan stress (σ_{pre}^{new}) and applied stress at different temperatures

3.2 Volume fraction dependence of steady-state creep rate

Figure 5(a) shows the relationships of the steady-state creep rate and the applied stress for the present nickel-base superalloys at different precipitate volume fractions (f). Apparently, the precipitation volume fraction governs the steady-state creep rate, and the steady-state creep rate deviations between the situation of f=0.2 and f=0.4 increases with increasing the applied stress.

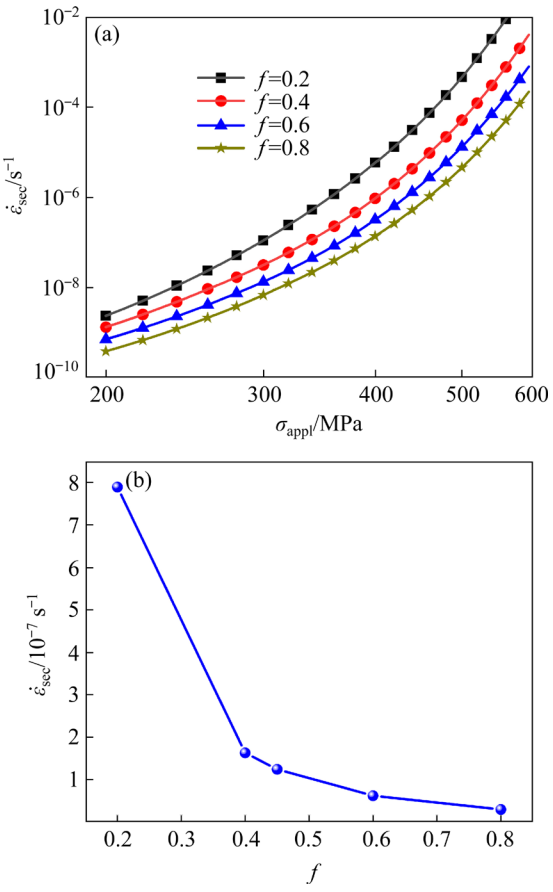

Fig. 5 Relationship between steady-state creep rate and applied stress at different precipitate volume fractions (a) and steady-state creep rate as function of precipitate volume fraction at σ_{appl} = 350 MPa (b)

In addition, when the applied stress is equal to 350 MPa, there is a negative correlation between the steady-state creep rate and the precipitate volume fraction, as shown in Fig. 5(b). The gross area of the precipitation and matrix interfaces increases with increasing the precipitate fraction, and consequently, the threshold stress increases. When volume fraction of precipitate is smaller than 0.4, the steady-state creep rate decreases rapidly with precipitate volume fraction increasing even at a high stress. However, the decreasing tendency of steady-state creep rate reduces drastically when volume fraction of precipitate is larger than 0.4. The above situations about the decreasing trend of the steady-state creep rate with increasing the precipitate volume fraction are in good agreement with the previous conclusions [43,44]. As the volume fraction of the precipitates increases, the creep resistance of the material enhances, but the ductility decreases [45,46]. Therefore, there might be an optimal precipitate volume fraction coupling the creep resistance and the ductility to obtain higher performance of materials by the heat treatment in precipitation-strengthening alloys.

As shown in Fig. 6, the critical precipitate radius and the new Orowan stress as a function of the applied stress are calculated by our model in a larger range of volume fractions. A slight reduction of the precipitate volume fraction causes a large change for the critical radius in low precipitate volume fraction, but a small change in high precipitate volume fraction. Moreover, Fig. 6(a) illustrates the asymptotic behavior in the critical precipitate radius which approaches a constant at high-applied stress with increasing the applied stress. Similarly, the new Orowan stress also exhibits asymptotic behavior, as shown in Fig. 6(b), owing to the significant effect of the critical precipitate radius on the new Orowan stress based on Eq. (14).

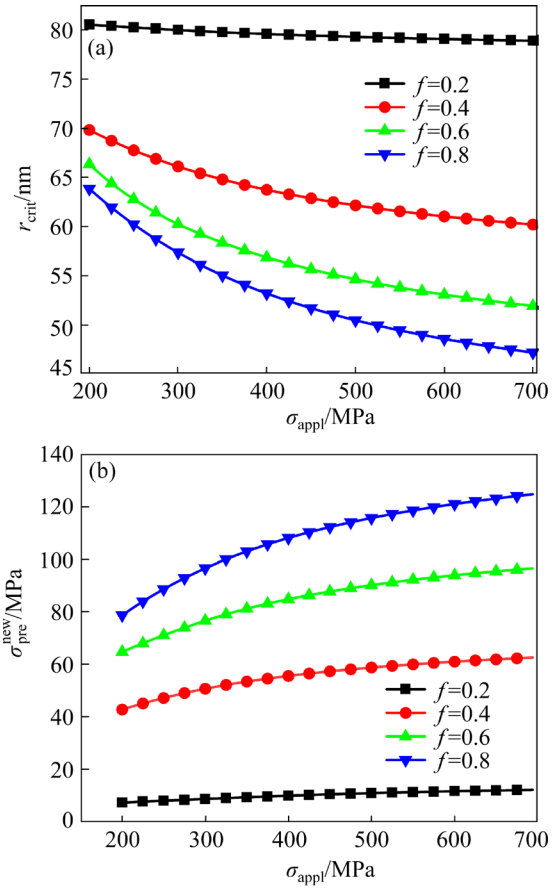

Fig. 6 Variation of critical precipitate radius (r_{crit}) (a) and new Orowan stress (b) with applied stress at different precipitate volume fractions

3.3 Applicability of model over wide temperature range

To investigate the effect of temperature on the steady-state creep rate, Fig. 7(a) shows the steady-state creep rate with temperature ranging from 700 to 1000 °C. It is found that the change of steady-state creep rate is negligible at medium or low temperature, but it drastically increases at high temperature. The precipitation is relatively stable when the temperature is lower than 875 °C. Furthermore, the precipitation with a smaller radius will gradually dissolve when the temperature is higher than 875 °C. In addition, the rafting of the precipitates with a larger radius occurs rapidly at the temperature higher than 875 °C. The rafting of the precipitates with a larger radius occurs rapidly at the temperature higher than 875 °C. The stress exponent increases with temperature decreasing, which is in reasonable agreement with the previous conclusion, as shown in Fig. 3(b) [20]. The dislocation mobility in Eq. (4) increases with temperature decreasing, which attributes to the strain-induced increase in vacancy concentration at higher temperatures. The results indicate that temperature is the key factor governing creep rate, especially at high applied stress. In Fig. 7(b), the ratio between the new Orowan stress in Eq. (14) to the classical Orowan stress in Eq. (5), is given as a function of the temperature. The ratio varies between 0.27 and 0.32 at σ_{appl}=400 MPa. It is

evident that the classical Orowan stress strongly overestimates the threshold stress. The classical Orowan stress includes the contribution of all precipitates, but in fact only a part of precipitates produces threshold stress. Moreover, as the temperature rises, the influence of applied stress on the ratio gradually decreases.

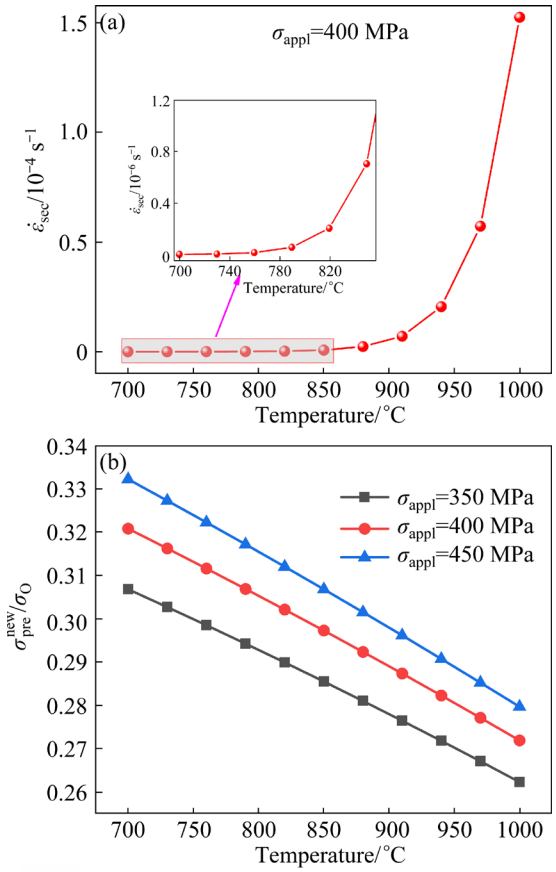

Fig. 7 Steady-state creep rate as function of temperature (a) and ratio of new Orowan stress to classical Orowan stress (σ_O) vs temperature (b)

Figure 8 indicates the linear decrease of the new Orowan stress and the critical precipitate radius with increasing temperature when the applied stress is equal to 400 MPa. Interestingly, this phenomenon is inconsistent with the situation of the opposite trend of critical precipitate radius and new Orowan stress, as shown in Fig. 6. This is because the shear modulus decreases as the temperature increases, which will reduce new Orowan stress. Moreover, the reduction in the radius of the precipitation causes the enhancement of new Orowan strengthening. But the critical precipitate radius changes only from 62.5 to 60.5 nm in a temperature range of 700−1000 °C, indicating that temperature only slightly affects the critical precipitate radius, as shown in Fig. 8. In addition, compared with the critical precipitate radius, the shear modulus exhibits a greater influence on Orowan stress in a wide range of temperatures. One key advantage of the present model is that it can be used to explain that the threshold stress decreases with temperature increasing.

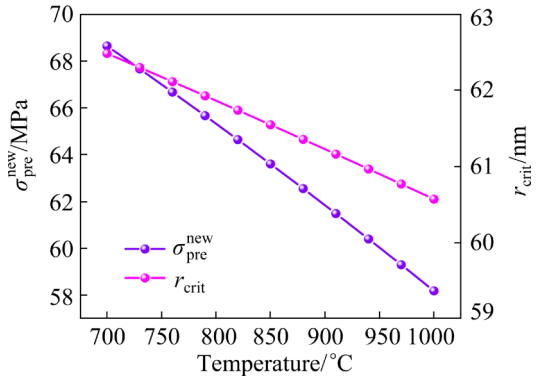

Fig. 8 New Orowan stress and critical precipitate radius as function of temperature at σ_{appl}=400 MPa

4 Conclusions

(1) The new creep model is established based on the synergetic modes of Orowan bypassing and climbing mechanisms for the dislocation−precipitate interaction in precipitation-strengthening alloys. Based on the new model, the contribution of precipitation to steady-state creep rate can be precisely predicted, and the results agree well with experimental data in a wide range of the applied stress.

(2) The present model also obtains the quantitative relationship between threshold stress and temperature, challenging the conventional view that the threshold stress is only related to the microstructures. Moreover, this enables all parameters of the present model to be obtained directly from experiments, with no need for empirical fitting. This addresses an important flaw in existing creep models.

(3) It is found that a slight reduction of the precipitate volume fraction causes a large change for the critical radius in low precipitate volume fraction, but a small change in high precipitate volume fraction. Meanwhile, the change of steady-state creep rate is negligible at medium or low temperature, but it drastically increases at high temperature.

CRediT authorship contribution statement

Fang LI: Conceptualization, Formal analysis, Software, Investigation, Data curation, Writing − Original draft; **Ding-ling YUAN:** Formal analysis, Software, Investigation, Data curation; **Kang-hua CHEN:** Formal analysis, Software; **Song-yi CHEN:** Conceptualization, Methodology, Validation, Writing − Review & editing, Supervision, Funding acquisition; **Li LI:** Conceptualization, Methodology, Validation, Writing − Review & editing, Supervision.

Declaration of competing interest

The authors declare that they have no known competing financial interests or personal relationships that could have appeared to influence the work reported in this paper.

Acknowledgments

The authors are grateful for the financial supports from the National Key Laboratory of Science and Technology for National Defence on High-Strength Lightweight Structural Materials of China (No. 20190104), State Key Laboratory of High-Performance Complex Manufacturing of Central South University, China (No. ZZYJKT2020-03), and the National Key Research and Development Program of China (No. 2016YFB0300801).

References

[1] QUAN Guo-zheng, ZHANG Yu-qing, ZHANG Pu, MA Yao-yao, WANG Wei-yong. Correspondence between low-energy twin boundary density and thermal-plastic deformation parameters in nickel-based superalloy [J]. Transactions of Nonferrous Metals Society of China, 2021, 31: 438−455.

[2] WU X, MAKINENI S K, LIEBSCHER C H, DEHM G, REZAEI M J, SHANTHRAJ P, GAULT B, BÜRGER D, EGGELER G, RAABE D. Unveiling the Re effect in Ni-based single crystal superalloys [J]. Nature Communications, 2020, 11: 1−13.

[3] CERVELLON A, HÉMERY S, KÜRNSTEINER P, GAULT B, KONTIS P, CORMIER J. Crack initiation mechanisms during very high cycle fatigue of Ni-based single crystal superalloys at high temperature [J]. Acta Materialia, 2020, 188: 131−144.

[4] WANG Kai-meng, JING Hong-yang, XU Lian-yong, ZHAO Lei, HAN Yong-dian, LI Hai-zhou, SONG Kai. Microstructure evolution of 55Ni−23Cr−13Co nickel-based superalloy during high-temperature cyclic deformation [J]. Transactions of Nonferrous Metals Society of China, 2021, 31: 3452−3468.

[5] PINZ M, WEBER G, LENTHE W C, UCHIC M D, POLLOCK T M, GHOSH S. Microstructure and property based statistically equivalent RVEs for intragranular γ−γ' microstructures of Ni-based superalloys [J]. Acta Materialia, 2018, 157: 245−258.

[6] KUMAR D, IDAPALAPATI S, WANG Wei, BHOWMIK A. Microstructural characteristics and strengthening mechanisms in a polycrystalline Ni-based superalloy under deep cold rolling [J]. Materials Science and Engineering A, 2019, 753: 285−299.

[7] GAO Shuang, SONG Zhen-feng, HE Bo, ZHOU Lan-zhang, HOU Jie-shan. Effect of Ta addition on solidification microstructure and element segregation of IN617B nickel-base superalloy [J]. Transactions of Nonferrous Metals Society of China, 2022, 32: 559−568.

[8] SHI J J, LI X, ZHANG Z X, CAO G H, RUSSELL A M, ZHOU Z J, LI C P, CHEN G F. Study on the microstructure and creep behavior of Inconel 718 superalloy fabricated by selective laser melting [J]. Materials Science and Engineering A, 2019, 765: 138282.

[9] LEE D H, SEOK M Y, ZHAO Y, CHOI I C, HE Jun-yang, LU Zhao-ping, SUH J Y, RAMAMURTY U, KAWASAKI M, LANGDON T G. Spherical nanoindentation creep behavior of nanocrystalline and coarse-grained CoCrFeMnNi high-entropy alloys [J]. Acta Materialia, 2016, 109: 314−322.

[10] ZHANG M, BROYLES S E, GIBELING J C. An improved description of creep in dispersion-strengthened metals [J]. Acta Materialia, 2020, 196: 384−395.

[11] LI J C M. A dislocation mechanism of transient creep [J]. Acta Metallurgica, 1963, 11: 1269−1270.

[12] DIETER G E, BACON D. Mechanical metallurgy [M]. New York: McGraw-hill. 1976.

[13] KASSNER M E. Fundamentals of creep in metals and alloys [M]. Oxford: Elsevier, 2015.

[14] NABARRO F R N, VILLIERS F L. Physics of creep and creep-resistant alloys [M]. CRC Press, 2018.

[15] COAKLEY J, DYE D, BASOALTO H. Creep and creep modelling of a multimodal nickel-base superalloy [J]. Acta Materialia, 2011, 59: 854−863.

[16] MARTIN J W. Precipitation hardening: Theory and applications [M]. Butterworth-Heinemann, 2012.

[17] LAGNEBORG R. Bypassing of dislocations past particles by a climb mechanism [J]. Scripta Metallurgica, 1973, 7: 605−613.

[18] SUI F, SANDSTRÖM R. Creep strength contribution due to precipitation hardening in copper–cobalt alloys [J]. Journal of Materials Science, 2019, 54: 1819−1830.

[19] ZHAO Ying-xin, FANG Qi-hong, LIU You-wen, WEN Pi-hua, LIU Yong. Creep behavior as dislocation climb over NiAl nanoprecipitates in ferritic alloy: The effects of interface stresses and temperature [J]. International Journal of Plasticity, 2015, 69: 89−101.

[20] ARZT E, ASHBY M F. Threshold stresses in materials containing dispersed particles [J]. Scripta Metallurgica, 1982, 16: 1285−1290.

[21] SANDSTRÖM R, HALLGREN J. The role of creep in stress strain curves for copper [J]. Journal of Nuclear Materials, 2012, 422: 51−57.

[22] VUJIC S, SANDSTRÖM R, SOMMITSCH C. Precipitation evolution and creep strength modelling of 25Cr20NiNbN austenitic steel [J]. Materials at High temperatures, 2015, 32: 607−618.

[23] SANDSTRÖM R. Fundamental models for creep properties of steels and copper [J]. Transactions of the Indian Institute of Metals, 2016, 69: 197−202.

[24] SANDSTRÖM R, FAROOQ M, ZUREK J. Basic creep models for 25Cr20NiNbN austenitic stainless steels [J]. Materials Research Innovations, 2013, 17: 355−359.

[25] HE Jun-jing, SANDSTRÖM R. Basic modelling of creep rupture in austenitic stainless steels [J]. Theoretical and

Applied Fracture Mechanics, 2017, 89: 139−146.
[26] BIELER T R, MUKHERJEE A K. The high strain rate superplastic deformation mechanisms of mechanically alloyed aluminum IN90211 [J]. Materials Science and Engineering A, 1990, 128: 171−182.
[27] BLUM W, REPPICH B. Creep of particle-strengthened alloys [M]. Aldershot: Pineridge Press, 1985.
[28] ELIASSON J, GUSTAFSON Å, SANDSTRÖM R. Kinetic modelling of the influence of particles on creep strength [J]. Key Engineering Materials, 2000, 171: 277−284.
[29] MAGNUSSON H, SANDSTRÖM R. The role of dislocation climb across particles at creep conditions in 9 to 12 pct Cr steels [J]. Metallurgical and Materials Transactions A, 2007, 38: 2428−2434.
[30] SANTOS-GÜEMES R, ESTEBAN-MANZANARES G, PAPADIMITRIOU I, SEGURADO J, CAPOLUNGO L, LLORCA J. Discrete dislocation dynamics simulations of dislocation−θ' precipitate interaction in Al−Cu alloys [J]. Journal of the Mechanics and Physics of Solids, 2018, 118: 228−244.
[31] GLADMAN T. Precipitation hardening in metals [J]. Materials Science and Technology, 1999, 15: 30−36.
[32] SHI D F, WANG C Y, CEPEDA-JIMENEZ C M, PÉREZ-PRADO M T. Atomic scale interactions of basal dislocations and twin boundaries with ultrathin precipitates in magnesium alloys [J]. Acta Materialia, 2021, 221: 117442.
[33] FANG Qi-hong, LI Li, LI Jia, WU Hong-yu, HUANG Zai-wang, LIU Bin, LIU Yong, LIAW P K. A statistical theory of probability-dependent precipitation strengthening in metals and alloys [J]. Journal of the Mechanics and Physics of Solids, 2019, 122: 177−189.
[34] AHMADI M R, POVODEN-KARADENIZ E, SONDEREGGER B, ÖKSÜZ K I, FALAHATI A, KOZESCHNIK E. A model for coherency strengthening of large precipitates [J]. Scripta Materialia, 2014, 84: 47−50.
[35] LI Fang, LI Li, FANG Qi-hong, LI Jia, LIU Bin, LIU Yong. The probability-correlative oxide particle strengthening in solid-solution alloys [J]. Journal of Materials Science, 2020, 55: 13414−13423.
[36] GALINDO-NAVA E I, CONNOR L D, RAE C M F. On the prediction of the yield stress of unimodal and multimodal γ' Nickel-base superalloys [J]. Acta Materialia, 2015, 98: 377−390.
[37] COLLINS D M, STONE H J. A modelling approach to yield strength optimisation in a nickel-base superalloy [J]. International Journal of Plasticity, 2014, 54: 96−112.
[38] OJO O A, RICHARDS N L, CHATURVEDI M C. Microstructural study of weld fusion zone of TIG welded IN 738LC nickel-based superalloy [J]. Scripta Materialia, 2004, 51: 683−688.
[39] BASOALTO H, SONDHI S K, DYSON B F, MCLEAN M. A generic microstructure-explicit model of creep in nickel-base superalloys [J]. Superalloys, 2004, 1: 897−906.
[40] BALIKCI E, RAMAN A, MIRSHAMS R A. Tensile strengthening in the nickel-base superalloy IN738LC [J]. Journal of Materials Engineering and Performance, 2000, 9: 324−329.
[41] SINHA N K. Short strain relaxation/recovery tests for evaluating creep response of nickel-base superalloys like IN-738LC [J]. Journal of Materials Science Letters, 2001, 20: 951−953.
[42] WOLLGRAMM P, BUCK H, NEUKING K, PARSA A B, SCHUWALOW S, ROGAL J, DRAUTZ R, EGGELER G. On the role of Re in the stress and temperature dependence of creep of Ni-base single crystal superalloys [J]. Materials Science and Engineering A, 2015, 628: 382−395.
[43] SUN Z, LIEBSCHER C H, HUANG S, TENG Z, SONG G, WANG G, ASTA M, RAWLINGS M, FINE M E, LIAW P K. New design aspects of creep-resistant NiAl-strengthened ferritic alloys [J]. Scripta Materialia, 2013, 68: 384−388.
[44] TENG Z K, LIU C T, GHOSH G, LIAW P K, FINE M E. Effects of Al on the microstructure and ductility of NiAl-strengthened ferritic steels at room temperature [J]. Intermetallics, 2010, 18: 1437−1443.
[45] LACERDA J C, CÂNDIDO L C, GODEFROID L B. Effect of volume fraction of phases and precipitates on the mechanical behavior of UNS S31803 duplex stainless steel [J]. International Journal of Fatigue, 2015, 74: 81−87.
[46] ANDERSON M, THIELIN A L, BRIDIER F, BOCHER P, SAVOIE J. δ phase precipitation in Inconel 718 and associated mechanical properties [J]. Materials Science and Engineering A, 2017, 679: 48−55.

协同 Orowan 绕过和攀移机制的镍基高温合金蠕变新模型

李 昉[1]，袁丁玲[2]，陈康华[1,2]，陈送义[2]，李 理[3]

1. 中南大学 粉末冶金国家重点实验室，长沙 410083；
2. 中南大学 轻合金研究院，长沙 410083；
3. 湖南大学 机械与车辆工程学院 汽车车身先进设计制造国家重点实验室，长沙 410082

摘 要：提出一种用于准确便捷预测析出相增强镍基高温合金稳态蠕变速率的蠕变新模型。基于析出相的空间分布，采用概率依赖的方法将位错−析出相交互作用中 Orowan 绕过和位错攀移机制的协同模式耦合到新的蠕变模型中。结果表明，新模型预测的稳态蠕变速率与实验数据吻合很好。此外，当前模型不再依赖于可调参数；同时，确定了阈值应力与温度的定量关系。这项工作为蠕变变形过程中位错−析出相交互作用提供新思路，并为设计具有更优异蠕变性能的析出强化合金提供有效模型。

关键词：镍基高温合金；蠕变模型；稳态蠕变速率；阈值应力

(Edited by Bing YANG)